Electrostatic Decay of Beam-generated Plasma Turbulence

Alberto M. Vásquez [1] and Daniel O. Gómez[1]

Instituto de Astronomía y Física del Espacio,
CC 67 - Suc 28, (1428) Ciudad de Buenos Aires, Argentina.

albert@iafe.uba.ar

ABSTRACT

The study of the evolution of a suprathermal electron beam traveling through a background plasma is relevant for the physics of solar flares and their associated type III solar radio bursts. As they evolve guided by the coronal magnetic field-lines, these beams generate Langmuir turbulence. The beam-generated turbulence is in turn responsible for the emission of radio photons at the second harmonic of the local plasma frequency, which are observed during type III solar radio bursts. To generate the radio emission, the beam-aligned Langmuir waves must coalesce, and therefore a process capable of re-directioning the turbulence in an effective fashion is required. Different theoretical models identify the electrostatic (ES) decay process $L_1 \rightarrow L_2 + S$ (L: Langmuir wave; S: Ion-acoustic wave) as the re-directioning mechanism for the L waves. Two different regimes have been proposed to play a key role: the back-scattering and the diffusive (small angle) scattering. This paper is a comparative analysis of the decay rate of the ES decay for each regime, and of the different observable characteristics that are expected for the resulting ion-acoustic waves.

Subject headings: Sun: corona — Turbulence — Sun: radio radiation

1. Introduction

During solar flares, large amounts of energy are released and transformed in coronal heating and particle acceleration, where regions of magnetic reconnection are believed to be the acceleration sites for suprathermal electron beams. Once accelerated, these beams travel through the coronal plasma guided by the coronal magnetic field-lines, and generating

[1]Also at the Department of Physics of the University of Buenos Aires, Argentina.

a variety of observable emissions. One long standing discrepancy in the modeling of this phenomena is that a beam with a given energy flux seems not to be able to simultaneously reproduce the observed emissivities in HXR (due to non-thermal bremsstrahlung at the chromosphere) and radio emission (due to beam-generated Langmuir turbulence in the corona). Once the beam energy flux is set to reproduce the HXR levels, the derived radio emissivities tend to be much higher than observed levels (Emslie & Smith 1984; Hamilton & Petrosian 1987).

In this context, we have developed a model for the evolution of electron beams and the generation of Langmuir turbulence, and we have also computed the emission of radio waves due to the coalescence of the beam-excited Langmuir waves. Our models describe the evolution of the beam and the produced Langmuir turbulence, consistently considering the effect of both collisions and quasi-linear wave-particle interaction. The level of turbulence derived from our models is up to two orders of magnitude lower than previous attempts (Vásquez & Gómez 1997). The production of photons at the second harmonic of the plasma frequency (radio waves), is the result of the coalescense ot two Langmuir waves. In our model we *assume* that the beam-generated Langmuir waves become isotropic in an effective way, due to electrostatic decay $L_1 + L_2 \rightarrow T(2\omega_{\rm pe})$. We found that an adequate treatment of the second harmonic photons generation (relaxing the head-on approximation) yields to further reductions of the radio emission (Vásquez et al. 2002). Although these results help to reduce the gap between the predicted HXR and radio emissivities, we find that further reductions are required.

The observed radio emission requires the coalescense of the beam-generated Langmuir waves. Therefore, a process capable of re-directioning the turbulence in an effective fashion is required. Different models in the literature resort to the electrostatic (ES) decay $L_1 \rightarrow L_2 + S$ (L: Langmuir wave; S: Ion-acoustic wave) as the re-directioning mechanism for the L waves. Two different regimes have been proposed to play a key role. One of them is the so called *back-scattering* limit of the ES decay (Edney & Robinson 2001; Cairns 1987). In this limit, the primary Langmuir wave decays into another one that propagates almost in the opposite direction. The other asymptotic regime is the *small-angle* limit of the ES decay, which has also been pointed out by some authors as potentially relevant in this context (Melrose 1982; Tsytovich 1970). In this limit, the propagation directions of both Langmuir waves (L_1 and L_2) form a small angle, and the ES decay acts on the beam-generated Langmuir waves as a difussion mechanism through **k**-space. In our models described above, the isotropization of Langmuir waves has been an assumption rather than a result obtained from our beam-turbulence quasi-linear equations. If the timescale of the ES decay is short enough (as compared to the timescale for the Langmuir waves to escape their generation region), it is reasonable to expect that the small-angle limit will render the

beam-generated Langmuir turbulence isotropic. In this work we revise this approximation in detail. We compare the rate of ion-acoustic wave generation in both limits, for a given set of beam-generated Langmuir spectra. We also analize the resulting frequencies of the ion-acoustic waves produced in each limit, and compare against reported in-situ observations.

In-situ observations of type III solar radio bursts have shown clear evidence in support of the ocurrence of the ES decay simultaneously with Langmuir waves. For example, Cairns & Robinson (1995) have analyzed ISEE 3 data that shows the coexistence of high and low frequency electrostatic waves, identified as Langmuir and ion-acoustic waves respectively, during a type III radio event. They analyze the observed low frequency waves, and find that their frequencies are consistent with those predicted by assuming the existence of the ES decay acting in the back-scattering limit. Similar observational works by Thejappa et al. (2003) and Thejappa & MacDowall (1998), analyzing URPE/*Ulysses* data, also support the occurence of the ES decay in association to impulsive Langmuir waves excited during type III radio events. In the present paper we make a similar analysis to the one by Cairns & Robinson (1995), and find out that the URPE data analyzed by Thejappa & MacDowall (1998) and Thejappa et al. (2003) is consistent with the occurrence of the ES decay acting in the diffusive limit.

This paper is organized as follows. In section 2 we revisit the ES decay and the general expression of its rate of occurrence. In section 3 we apply the general results to the specific case of a beam-generated Langmuir spectrum. We make a quantitative comparison between the diffusive and back-scattering cases. In section 4 we compute the expected frequencies for the generated ion-acustic waves for the particular type III solar radio bursts observed and studied by Thejappa & MacDowall (1998) and Thejappa et al. (2003). Finally, in section 5 we list our main conclusions.

2. Electrostatic Decay Rate

The electrostatic decay $L_1 \rightarrow L_2 + S$ (where $L_{1,2}$: Langmuir; S: Ion-acustic), must verify the momentum and energy conservation, so that their wave vectors and frequencies satisfy

$$\mathbf{k}_{L1} = \mathbf{k}_{L2} + \mathbf{k}_S \quad ; \quad \Omega_{L1} = \Omega_{L2} + \Omega_S \tag{1}$$

where the dispersion relationships are,

$$\Omega_L(\mathbf{k}_L) \approx \omega_{\rm pe}\left(1+\frac{3}{2}(k_L\lambda_{\rm De})^2\right) \;\; ; \;\; \Omega_S(\mathbf{k}_S) \approx k_S V_S \tag{2}$$

From these relations, we obtain the modulus and direction of the wave vectors of the resulting waves L_2 and S (see Figure 1), with respect to the wave vector of the initial Langmuir wave L_1

$$\cos(\alpha) \equiv \frac{\mathbf{k}_{L1}\cdot\mathbf{k}_{L2}}{k_{L1}k_{L2}} = \frac{k_{L1}-\mu\ k_S}{k_{L2}} \tag{3}$$

$$\mu \equiv \cos(\beta) = \frac{\mathbf{k}_{L1}\cdot\mathbf{k}_S}{k_{L1}k_S} = \frac{k_S+2k_0}{2k_L} \;\; ; \;\; k_0 \equiv \frac{1}{3}\frac{\omega_e}{V_{\rm Te}}\sqrt{\frac{m_e}{m_i}} \tag{4}$$

$$k_{L2}^2 = k_{L1}^2 - 2k_0k_S \tag{5}$$

The spectral density $N_{\mathbf{k}}^{\sigma}$ of the plasmons of type σ (with $\sigma = L,\ S$ in this case), is defined such that the volumetric density of plasmons is $n^{\sigma} = \int \frac{d\mathbf{k}}{(2\pi)^3}\ N_{\mathbf{k}}^{\sigma}$. In terms if these spectral densities, the rate of production of ion-acoustic (S) waves is (Tsytovich 1970)

$$\frac{dN_{\mathbf{k}_S}^S}{dt} = \int \frac{d\mathbf{k}_{L1}d\mathbf{k}_{L2}}{(2\pi)^6} w_L^{SL} \times \left[N_{\mathbf{k}_{L1}}^L N_{\mathbf{k}_S}^S + N_{\mathbf{k}_{L1}}^L N_{\mathbf{k}_{L2}}^L - N_{\mathbf{k}_{L2}}^L N_{\mathbf{k}_S}^S\right] \tag{6}$$

where the probability of the decay is

$$w_L^{SL} = \frac{\hbar e^2\Omega_S^3 m_p(2\pi)^6}{8\pi m_e^3 V_{\rm Te}^4 k_S^2}\left[\frac{\mathbf{k}_{L1}\cdot\mathbf{k}_{L2}}{k_{L1}k_{L2}}\right]^2 \delta(\mathbf{k}_{L1}-\mathbf{k}_{L2}-\mathbf{k}_S)\times \delta(\Omega_{L1}-\Omega_{L2}-\Omega_S) \tag{7}$$

where $m_e,\ m_p$ are the electron and proton mass respectively, $V_{\rm Te}$ is the electron thermal velocity, and the delta functions express the momentum and energy conservation.

3. Results for beam-generated Langmuir waves

We use the expresions of the previous section to compute the decay rate of a beam-generated Langmuir spectrum. Hereafter we adopt a given shape for a beam generated

Langmuir spectrum. The dependence of the spectrum upon the modulus of wavenumber, has been obtained by Vásquez & Gómez (1997). We also assume this spectrum to by axisymmetric and with a gaussian angular spread about the direction of the beam, and analyze the *initial* ES decay rates.

The beam-generated Langmuir turbulence is initially aligned with the beam propagation axis (the local magnetic field). As it proceeds, we expect the ES decay to re-directionate the Langmuir waves. We thus divide our analysis in two cases. In a first place we analyze the ES decay of a perfectly colimated Lanmguir spectrum. Later on, we analize the same rates for a non-colimated spectrum. In both stages of our analysis we compute and compare the rates for both difussive and back-scattering cases.

3.1. Colimated Langmuir spectra

Let us evaluate the initial rate of production of S waves generated by a Langmuir spectrum, which is in turn produced by a perfectly colimated beam (i.e. we take $N^L_{\mathbf{k}_{L2}} = 0$),

$$\frac{1}{\tau(\mathbf{k}_S)} \equiv \frac{1}{N^S_{\mathbf{k}_S}} \frac{dN^S_{\mathbf{k}_S}}{dt} \approx \int \frac{d\mathbf{k}_{L1} d\mathbf{k}_{L2}}{(2\pi)^6} w^{SL}_L N^L_{\mathbf{k}_{L1}} = \frac{K(T_e, n_e)}{(2\pi)^3} \int \frac{d\mathbf{k}_{L1}}{(2\pi)^3} \frac{\left[\mathbf{k}_{L1} \cdot (\mathbf{k}_{L1} - \mathbf{k}_S)\right]^2}{k^2_{L1} (\mathbf{k}_{L1} - \mathbf{k}_S)^2} N^L_{\mathbf{k}_{L1}} \delta\left(k_1 \mu - \frac{k_s + 2k_0}{2}\right) \tag{8}$$

where the integral in $\mathbf{k}_{L2}$ has been performed using the momentum conservation, and the function K is given by

$$K(T_e, n_e) = \frac{\hbar e^2 \Omega^3_S m_i (2\pi)^6}{8\pi m^3_e V^4_{\rm Te} k^2_S} \frac{\omega_{\rm pe}}{3 k_S V^2_{\rm Te}} \tag{9}$$

In a previous work (Vásquez & Gómez 1997; Vásquez et al. 2002) we developed a model to derive the spectrum of beam-generated Langmuir waves. According to this model, the wavenumber of the excited Langmuir waves lays in the range

$$k_1 = [k_{\rm min}, k_{\rm max}] \approx [6, 12]\ k_0\ \sqrt{T_6} \tag{10}$$

where $T_6 \equiv T_e[{\rm K}]/10^6$. Approximating to a constant level for the perfectly colimated spectrum, and calling $\mathbf{e}_{\rm Z}$ to the direction of the beam,

$$N^L_{\mathbf{k}_{L1}} = (2\pi)^3 \frac{n^L}{\Delta k^L} \delta(k_{1x})\delta(k_{1y}), \tag{11}$$

where Δk^L is the spectral width, the result for the initial production rate of ion-acoustic waves is

$$\frac{1}{\tau(\mathbf{k}_S)} = \frac{1}{\tau_0}\ P(k_S,\mu) \tag{12}$$
$$\frac{1}{\tau_0} \equiv \frac{\pi}{4}\frac{k_0}{\Delta k^L}\frac{\omega_{\rm pe} W^L}{n_e m_e V^2_{\rm Te}}$$

where the dimensionless function $P(k_S,\mu)$ is given by

$$P(k_S,\mu) \equiv \frac{1}{\mu}\ \frac{\left[2+(k_S/k_0)(1-2\mu^2)\right]^2}{4+(k_S/k_0)^2+4(k_S/k_0)(1-2\mu^2)};\ \ \text{if}\ \ 6\sqrt{T_6} < \frac{k+2k_0}{2\mu} < 12\sqrt{T_6} \tag{13}$$

and is zero otherwise. Figure 2 shows the dimensionless decay rate $P(k_S,\mu)$ given by equation (13), as a function of the wave number k_S and the angle $\theta_{\mathbf{SL}}$ between $\mathbf{k}_S$ and $\mathbf{k}_L$. Here we have taken $T_6 = 0.17$ as a characteristic number for a type III solar radio bursts analyzed in section 4. This graphic confirms that the cases of maximum probability of occurrence are the back-scattering (with $\theta_{\mathbf{SL}} \to 0,\ P \sim 1$) and the diffusive scattering (with $\theta_{\mathbf{SL}} \sim 75^\circ,\ P \sim 4$). The factor of four in the diffusive decay rate results from the modulation factor $1/\mu$ in equation (13). The propagation direction of the resulting ion-acoustic wave is parallel to the beam propagation in the case of back-scattering, and almost perpendicular to the beam in the diffusive case (with $k_S \ll k_L$). We therefore find that the decay rate becomes maximum for two limiting cases: a) small-angle (diffusive) scattering: $\alpha \to 0$, and b) back-scattering: $\alpha \to \pi$.

Under the diffusive scattering approximation, estimates for the characteristic isotropization and energy transfer timescales, indicate that the latter is much larger, implying that the isotropization occurs in a quasi-elastic fashion Tsytovich (1970) (see also Vásquez et al. 2002). The quasi-conservation of the total energy is readily seen from the following argument. The ES decay conserves the total number of Langmuir plasmons. Now, given the weak dependence of their energy on the wave-number (see equation (2)), we can approximate the energy of each plasmon as $\omega_{\rm pe}$. Therefore, this decay can not produce a significant change in the total Langmuir wave energy.

3.2. Non-colimated Langmuir spectra

In the previous section we found that the ES decay of the 1D Langmuir spectrum generated by a perfectly colimated beam is initially dominated by small-angle decay processes and, in second place, by back-scattering. We then expect that after a transient stage, the Langmuir spectrum is not longer perfectly aligned with the beam direction, and that a growing back-scattered spectrum also arises. Nonetheless, we expect that the forward spectrum will contain much more energy than the backward spectrum, at least during the early stages of the evolution. Under this assumption, we consider now an axisymmetric spectrum around the beam direction, and model it through functions $N_{\mathbf{k}} = N(\theta, k)$ that peak in the forward direction and monotonically decrease as $\theta \to \pi$.

Let us start by analyzing the small angle scattering limit, i.e. $k_S \ll k_L$. For the diffusive decay we have that the spectral width of the ion-acoustic waves produced is much smaller than the spectral width of the primary Langmuir waves. More specifically, we have

$$\frac{\Delta k_S}{\Delta k_L} \sim 3\frac{\langle k_S \rangle}{\langle k_L \rangle} \ll 1 \tag{14}$$

where $\langle k_S \rangle = k_{S\max}/2$ and $\langle k_L \rangle = (k_{\min} + k_{\max})/2$ indicate mean wavenumber values. As the decay proceeds, each ES decay process will produce one ion-acoustic wave, hence

$$N^L \Delta k_L \sim N^S \Delta k_S \to \frac{N^L}{N^S} \sim \frac{\Delta k_S}{\Delta k_L} \ll 1 \tag{15}$$

i.e. the *spectral* density of the (emitting) Langmuir waves becomes much lower than that of the (emitted) ion-acoustic waves (even though the Langmuir energy density can be much larger than that of the ion-acoustic waves). Thus, we neglect the term $N^L N^L$ in the decay rate given by equation (6) and approximate

$$\begin{aligned} \frac{1}{\tau(\mathbf{k}_S)} \equiv \frac{1}{N^S_{\mathbf{k}_S}} \frac{dN^S_{\mathbf{k}_S}}{dt} \approx \int \frac{d\mathbf{k}_{L1} d\mathbf{k}_{L2}}{(2\pi)^6}\, w_L^{SL} \left(N^L_{\mathbf{k}_{L1}} - N^L_{\mathbf{k}_{L2}}\right) = \\ \frac{K}{(2\pi)^6} \int d\mathbf{k}_{L1} \frac{\cos^2(\alpha)}{\mu} \left(N^L_{\mathbf{k}_{L1}} - N^L_{\mathbf{k}_{L2}}\right)\, \delta\left(k_{L1} - \frac{2k_0 + k_S}{2\mu}\right) \end{aligned} \tag{16}$$

where K is given by equation (9) (see also equation (8)). Using the energy conservation, equation (17) reduces to the double integral,

$$\frac{1}{\tau(\mathbf{k}_S)} \approx \frac{K}{(2\pi)^6}\int_0^{2\pi} d\phi_1 \int_0^{\pi} d\theta_1 \ \sin\theta_1 \ \left[\frac{k_1^2 \cos^2(\alpha)}{\mu}\left(N(k_1,\theta_1) - N(k_2,\theta_2)\right)\right]_{k_1=(k_S+2k_0)/(2\mu)} \tag{17}$$

where we have assumed the Langmuir spectrum $N_{\mathbf{k}}$ to be symmetric about the beam propagation axis $\mathbf{e}_{\mathrm{Z}}$ (i.e. independent of the angle ϕ), and the values k_2, θ_2 are related to k_1, θ_1 through

$$k_2 = \sqrt{k_1^2 - 2k_0 k_1} \tag{18}$$

$$\cos(\theta_2) = \frac{(\mathbf{k}_{L1} - \mathbf{k}_S)\cdot \mathbf{e}_{\mathrm{Z}}}{k_2} \tag{19}$$

and $\cos(\alpha)$ is given by equation (3). We note here that in the back-scattering limit, the term $N_{L1}N_{L2}$ can not be neglected. Instead, for back-scattering, we expect that $N_{L2} \ll N_{L1}$ (at early stages of the evolution), and hence we can neglect the two last terms in equation (6). Therefore, the rate for back-scattering can be obtained from equation (17) by simply neglecting the second term N_{θ_2}, and also taking the limits $\cos(\alpha) \to -1$ and $\mu \to +1$.

To compare these rates against the perfectly colimated case (equation (12)), let us multiply and divide the RHS of equation (17) by $K_1 \equiv (2\pi)^3 n_L/\Delta k_L$, to obtain

$$\frac{1}{\tau(\mathbf{k}_S)} = \frac{1}{\tau_0} P_1(k_S, \theta_S) \tag{20}$$

where $1/\tau_0$ is the reference rate given by equation (12), θ_S is the angle between the ion acoustic wave vector and the beam propagation direction $\mathbf{e}_{\mathrm{Z}}$, and the dimensionless function $P_1(k_S, \theta_S)$ is given by

$$P_1(k_S,\theta_S) = \frac{\Delta k_L}{n_L}\frac{1}{(2\pi)^3}\int_0^{2\pi} d\phi_1 \int_0^{\pi} d\theta_1 \ \sin\theta \ \left[\frac{k_1^2 \cos^2(\alpha)}{\mu}\left(N(k_1,\theta_1) - N(k_2,\theta_2)\right)\right]_{k_1=(k_S+2k_0)/(2\mu)} \tag{21}$$

We use this expression to evaluate the decay rate for a spectral model that is stronger in the forward direction (but not colimated). Here we neglect the dependence in wavenumber, and assume the spectral density as constant within the range $[k_{\min}, k_{\max}]$ given by equation (10). More specifically we consider

$$N(k,\theta) = C\frac{1+e^{-\theta_c/\Delta\theta}}{1+e^{(\theta-\theta_c)/\Delta\theta}}; \quad \text{if} \quad k_{\min} < k < k_{\max} \tag{22}$$

where the normalization constant C is such that the number density of Langmuir plasmons is $n^L = \int \frac{\mathbf{k}}{(2\pi)^3} N_{\mathbf{k}}$. As an example, Figure 3 shows this function for $\theta_c = 25^\circ,\ \Delta\theta = 2^\circ$. This angular distribution peaks at $\theta = 0$ and monotonically decreases with increasing θ. The mean value is reached at θ_c. Thus, for smaller values of this parameter the spectrum is more colimated. The parameter $\Delta\theta$ measures the half-width over which the function varies from 75% to 25% of its maximum value. For smaller values of this parameter, the spectrum has a sharper angular edge.

Figure 4 shows the resulting P_1 for two sharp-edged angular spectra with $\Delta\theta = 2^\circ$. One spectrum is well concentrated along the beam direction with $\theta_c = 5^\circ$, and the other corresponds to a wider distribution with $\theta_c = 25^\circ$. Our expression for P_1 (equation (21)) is valid in the diffusive regime $k_S \ll k_L$, so we show results for $k_S = 0, .., \langle k_L \rangle /10$. Rates monotonically increase with k_S, until they saturate at about $\langle k_L \rangle /5$. For larger values of k_S the rates decrease with increasing k_S.

Higher rates are obtained for a more colimated beam, and the peak value is reached at a larger angle θ_S. This behaviour can be understood in terms of our analytic decay analysis for the perfectly colimated case. The peak is expected to occur as the result of the decay of Langmuir waves located in regions where the angular gradient of the spectrum is maximum, i.e. located around θ_c. This is because in this region the difference $N(k_1,\theta_1) - N(k_2,\theta_2)$ in equation (21) reaches its largest value. On the other hand, for the characteristic numbers of type III solar radio bursts being used in this analysis, our results (see Figure 2) show that the ion-acoustic waves are preferentially directed toward angles around the value $\theta_S \sim 75^\circ$ (with respect to the direction of the decaying Langmuir wave). We can therefore expect then that Langmuir waves with an angle θ_c respect to the $\mathbf{e}_Z$ axis will preferentially produce ion-acoustic waves with an angle $\theta_S \sim 75^\circ - \theta_c$. This rough estimate gives peak angles of 70°and 50° for the two values of θ_c considered here, which is in agreement with the detailed numerical results shown in Figure 4.

Also, in the perfectly colimated limit ($\theta_c \to 0,\ \Delta\theta \to 0$), from comparison with equation (13), we expect that peak values of P_1 will be close to the peak value $P \sim 4$ corresponding to the perfectly colimated case (see Figure 2). The numerical results of Figure 4 are consistent with this. As a consistency check, Figure 5 shows the same results for a highly colimated distribution with $\theta_c = 0.5^\circ,\ \Delta\theta = 0.5^\circ$, with peak rates of $P_1 = 3.5$, at $\theta_S \sim 74^\circ$.

For a fixed $k_S = \langle k_L \rangle /10$, Figure 6 shows the effect of reducing the Langmuir wave distribution angular gradient. For the distribution with the edge centered on the angle

$\theta_c = 5°$, left panel shows the resulting rates for $\Delta\theta = 2°,\ 10°$. The right panel shows the corresponding results for the distribution with edge on the angle $\theta_c = 25°$. The effect of a smoother distribution is to extend the possible angles of the produced ion-acoustic waves over a much wider range. Also, as the angular gradient of the Langmuir spectrum is reduced, the difference $N_1 - N_2$ in equation (21) decreases, and hence $P_1(\theta_S)$ yields lower values.

Let us also compare the different diffusive decay rates against the corresponding back-scattering decay rates. The backscattering of a Langmuir plasmon of wavenumber k_L produces an ion-acoustic plasmon of wavenumber $k_S = 2k_L - 2k_0$, as follows from taking the limit $\mu \to +1$ in equation (4). Figure 7 shows the resulting back-scattering P_1 for the same two Langmuir spectra analyzed in Figure 4. Thin curves correspond to $k_S = 2k_{L,min} - 2k_0$ and thick curves to $k_S = 2k_{L,max} - 2k_0$. In this case, being the result of back-scattering, the angular distribution of the decay rate closely follows that of the decaying Langmuir waves $N(k_1, \theta_1)$ in equation (21) (compare for example the right panel of Figure 7 with Figure 3).

A comparison between the back-scattering results of Figure 7 against the diffusive decay results Figure 4 shows that the diffusive rates are always larger, by factors of order 2 to 5. Figure 8 shows the same results for a highly colimated distribution with $\theta_c = 0.5°,\ \Delta\theta = 0.5°$. The resulting rates are of order $P_1 \sim 1.5$, or about a factor of 2 lower than the corresponding diffusive decay values of Figure 5. These results are consistent with the perfectly colimated beam results of Figure 2. Therefore we find that, in all cases, diffusive decay rates are systematically larger (though comparable) than the corresponding back-scattering rates.

4. Frequencies of the ion-acoustic Waves

Several space-based missions, located at distances of order 1 AU from the Sun, are designed to perform in-situ measurements of the extended solar wind. These missions are able then to perform in-situ measurements of type III solar radio bursts, that sometimes extend far away from the Sun and reach the Earth. One of these instruments is the *Unified Radio and Plasma Wave Experiment* (URAP) aboard the *Ulysses* mission. For the purpose of interpreting type III burst data collected by this experiment, let us suppose that an ion-acoustic wave travels through the region of the experiment. If $\mathbf{V}_{\rm sw}$ is the local solar wind velocity, the Doppler-shifted frequency of the ion-acoustic wave, as measured by the experiment, is given by

$$f_S \;=\; \frac{1}{2\pi}\left(k_S V_S + \mathbf{k}_S \cdot \mathbf{V}_{\rm sw}\right) =$$

$$= \frac{k_S}{2\pi}\left(V_S + V_{\rm sw}\,\cos\left(\theta_{\mathbf{Sr}}\right)\right) =$$
$$= 2\frac{f_{\rm pe}}{V_\phi}\left(\cos\left(\theta_{\mathbf{SL}}\right) - \frac{V_S V_\phi}{3V_{\rm Te}^2}\right)\left(V_S + V_{\rm sw}\,\cos\left(\theta_{\mathbf{Sr}}\right)\right) \quad (23)$$

where k_S has been eliminated from equation (4), $\theta_{\mathbf{SL}}$ and $\theta_{\mathbf{Sr}}$ are the angles between the propagation direction of the ion-acoustic wave and those of the primary (beam aligned) Langmuir waves, and the (radial) solar wind, respectively. This formula is analogous to the one used by Cairns & Robinson (1995) to analyze a type III solar radio burst. They assume the ES decay products only in the back-scattering limit, and hence they consider the particular case $\cos\left(\theta_{\mathbf{SL}}\right) = +1$. Also in that limit, the produced ion-acoustic waves propagate aligned with the beam direction, so that $\theta_{\mathbf{Sr}} = \theta_{\mathbf{Lr}}$, i.e. the angle between the primary Langmuir waves and the solar wind direction. On the other hand, in the diffusive limit, $\theta_{\mathbf{SL}} > 0$ so that the angle $\theta_{\mathbf{Sr}}$ takes the range of values $|\theta_{\mathbf{SL}} - \theta_{\mathbf{Lr}}| < \theta_{\mathbf{Sr}} < \theta_{\mathbf{SL}} + \theta_{\mathbf{Lr}}$.

To quantify the predicted frequencies for the ion-acoustic waves in each of these two limiting cases, we refer to a specific observational case, analyzed by Thejappa & MacDowall (1998). They show the data of a type III solar radio event recorded by URAP/*Ulysses* on March 14 1995. Their detailed analysis shows radio emissions at both the plasma and second harmonic frequencies. At the same time, impulsive electrostatic fluctuations were recorded at the local plasma frequency, which turns out to be $f_{\rm pe} \sim 23$ kHz, identified as Langmuir wave bursts. The WFA (Wave Form Analyzer) instrument detected electric fluctuations, highly correlated in time with the observed Langmuir impulsive peaks, in the range $0 \rightarrow 450$ Hz. The instrument also detected magnetic field fluctuations in the range $0 \rightarrow 50$ Hz. The combination of these facts indicates that the electric field fluctuations in the range $50 \rightarrow 450$ Hz are of a pure electrostatic nature, such as ion-acoustic waves. If this is the case, its strong temporal correlation with the Langmuir bursts supports the idea that the ion-acoustic waves may be produced by the ES decay of the L-waves (see also Cairns & Robinson 1995). On the other hand, below 50 Hz fluctuations are most likely of electromagnetic nature, such as whistlers. Summarizing, the analysis by Thejappa & MacDowall (1998) strongly suggests the presence of ion-acoustic waves in the range $50 \rightarrow 450$ Hz, for this particular event, and that these waves are produced as the result of the ES decay of the beam-excited Langmuir waves.

For the event under consideration, the numerical values of the relevant parameters are (Thejappa & MacDowall 1998): $V_{\rm S} = 5.1\times10^6$cm/seg, $V_{\rm Te} = 1.6\times10^8$cm/seg (corresponding to $T_e = 1.7\times10^5$K), $V_{\rm sw} = 3.4\times10^7$cm/seg, $V_\phi \sim V_{\rm beam} \pm 25\%$, with a mean beam velocity estimated to be $V_{\rm beam} = 3.5\times10^9$cm/seg, $f_{\rm pe} = 2.3\times10^4$Hz, $\theta_{\mathbf{Lr}} \sim 45^\circ$.

Using these numerical values we compute now, in the two limit cases under analysis, the

predicted ion-acoustic wave frequencies. In all cases, we assume that the primary (beam-excited) Langmuir waves form a mean angle $\theta_{\mathbf{Lr}} = 45^\circ$ with respect to the solar wind direction, and that the primary Langmuir waves have phase speeds in the range $V_\phi = V_{\rm beam} \pm 25\%$.

Figure 2 shows that, in the diffusive limit, decays proceed most likely for angles $\theta_{\mathbf{SL}}$ in the range $60^\circ \rightarrow 75^\circ$ (in this range the probability is about twice the back-scattering probability). Using this range of angles in equation (23), we find that the diffusive-scattering assumption yields ion-acoustic waves in the range 50 Hz $\rightarrow$ 215Hz. On the other hand, if back-scattering is assumed, we have $\theta_{\mathbf{SL}} = 0^\circ$, and equation (23) yields ion-acoustic frequencies in the range 215 Hz $\rightarrow$ 415 Hz. The difference between the predictions in both limits is due to the term $\left(\cos\left(\theta_{\mathbf{SL}}\right) - \frac{V_S V_\phi}{3V_{\rm Te}^2}\right)$, that is maximized in the back-scattering case as $\cos\left(\theta_{\mathbf{SL}}\right) \sim +1$.

If the the primary Langmuir waves form a variable angle $0^\circ < \theta_{\mathbf{Lr}} < 90^\circ$ with respect to the solar wind direction, the frequency ranges predicted in both limits overlap each other, within the observed range. In this case, the back-scattering limit yields predicted ion-acoustic frequencies over the whole observed range (as already pointed out by Thejappa & MacDowall 1998). We thus find that the predictions, for both asymptotic cases are consistent with the observations. Taking mean values of the different parameters, we find out that for the back-scattering assumption the predicted frequencies are consistent with the higher frequency portion of the observations (see also Cairns & Robinson 1995). On the other hand, the diffusive-scattering limit yields predicted frequencies that are consistent with the lower frequency portion of the observed electrostatic fluctuations.

Further empirical support arises from a recent observational work by Thejappa et al. (2003), where they analyze URAP data for another type III burst, in a similar fashion to the case already described. This case corresponds to in-situ observations at much larger heliocentric distances, specifically at 5.2 AU, where the local ambient plasma parameters are very different ($f_{\rm pe} \sim 2$ kHz, $T_e \sim 8.8 \times 10^4$K) to those of the previous case. The beam velocity (and hence the primary Langmuir waves phase velocity) is estimated to be $V_\phi \sim 1.5 \times 10^9$cm/seg $\pm$ 30%. In this other case, the WFA-URAP instrument also detected electric field fluctuations correlated in time with Langmuir bursts. The electric waves that can be safely assumed to be of electrostatic nature (i.e. with no simultaneous detection of magnetic field fluctuations above the background level) are in the frequency range 20 $\rightarrow$ 200 Hz.

We repeated our probability calculations for this case, and find out that, in the diffusive limit, decays proceed most likely for angles $\theta_{\mathbf{SL}}$ in the range $55^\circ \rightarrow 73^\circ$ (in this range the probability is about twice the back-scattering probability). Using this range of angles, in the diffusive limit, the predicted ion-acoustic frequencies result in the range 0Hz $\rightarrow$ 60 Hz. On the other hand, under the back-scattering assumption the predicted frequencies are in the

range 55 Hz → 105 Hz.

5. Conclusions

From the theoretical point of view, an analysis of the ES decay rate indicates that the process is dominated by two limiting cases: diffusive (small angle) scattering and back-scattering. We find that the decay rates are comparable for both cases, being the diffusive decay rates systematically larger than those of the back-scattering limit. Given the results of our quantitative comparative analysis, we believe that both limiting cases are acting at the same time. Furthermore, we speculate the net effect of diffusive decay and back-scattering acting simultaneously is then that of a diffusive isotropization of the beam-generated Langmuir spectrum. The back-scattering generates a backwards directed spectrum (respect to the beam propagation direction), but then this secondary spectrum can also diffuse by small-angle decay. Thus, if the ES decay is assumed to be present in solar flare and type III solar radio burst scenarios, we believe that its capability to isotropize Langmuir waves can not be neglected.

From an observational point of view, we refer to analyses of a type III bursts by Thejappa & MacDowall (1998) and Thejappa et al. (2003). They registered low frequency electrostatic fluctuations which are strongly correlated in time with impulsive Langmuir wave bursts. We find that the observed frequencies of these fluctuations are consistent with the predicted frequencies of ion-acoustic waves produced by the ES decay of the primary (beam-excited) Langmuir waves. Under the back-scattering assumption the predicted frequencies are consistent with the higher frequency portion of the observations. On the other hand, the diffusive-scattering limit yields predicted frequencies that are consistent with the lower frequency portion of the observed electrostatic fluctuations. The relative burst intensities at the two frequency ranges could then serve as a proxy for the relative effectiveness of the occurrence of the ES decay in both limits, that we anticipate to be comparable from our theoretical analysis.

From this analysis, we speculate that both the back-scattering and diffusive limits of the ES decay may be relevant in type III bursts (and presumably also in solar flare radio events). Also, the beam-generated Langmuir turbulence may become isotropic as the ES decay proceeds mainly in the two limit cases of diffusive scattering and back-scattering. We postpone for a future work the investigation of the coupling between the ES decay and the quasi-linear beam-turbulence interaction. We believe that the simultaneous consideration of both effects can bring HXR and radio emission predictions into a better agreement with observations. This is due to the fact that its inclusion will imply a limitation of the effective-

ness of the quasi-linear relaxation, yielding to lower Langmuir turbulence levels, and hence lower radio emissivity.

We thank the anonymous referee for useful suggestions that helped to clarify our main conclusions. This work was funded by the *Agencia Nacional de Promoción de Ciencia y Tecnología* (ANPCyT, Argentina) through grant 03-09483. We also thank *Fundación Antorchas* (Argentina) for partial support through grant 14056-20.

REFERENCES

Cairns, I.H. 1987, J. Plasma Phys., 39, 179

Cairns, I.H. & Robinson, P.A. 1995, ApJ, 453, 959

Edney, S.D. & Robinson, P.A. 2001, Phys. Plasmas, V.8 N.2, 428

Emslie, A.G. & Smith, D.F. 1984, ApJ, 279, 882

Hamilton, R.J. & Petrosian, V. 1987, ApJ, 321, 721

Melrose, D.B. 1982, Sol. Phys., 79, 173

Thejappa G., MacDowall R.J., Scime, E.E. & Littleton, J.E. 2003, J. Geophys. Res., 108, No. A3, 1139

Thejappa G. & MacDowall R. J. 1998, ApJ, 498, 465

Tsytovich, V.N. 1970, *Nonlinear Effects in Plasma*, New York: Plenum Press

Vásquez, A.M. & Gómez, D.O. 2003, Anales AFA, Vol. 14, 106

Vásquez, A.M., Gómez, D.O., & Ferro Fontán, C. 2002, ApJ, 564, 1035

Vásquez, A.M. & Gómez, D.O. 1997, ApJ, 484, 463

Fig. 1.— Momentum conservation in the electrostatic decay, $\mathbf{k}_{L1} = \mathbf{k}_{L2} + \mathbf{k}_S$. Angles α and β are given by equations (4) and (5).

Fig. 2.— Dimensionless decay rate $P(\mathbf{k}_S)$, as a function of $(k_S, \theta_{\mathbf{SL}})$.

Fig. 3.— Model for the angular distribution of the Langmuir spectrum, with $\theta_c = 25^\circ$ and $\Delta\theta = 2^\circ$. The vertical lines indicate the angles θ_c (full line), and $\theta_c \pm \Delta\theta$ (dashed lines).

Fig. 4.— Diffusive decay: dimensionless factor $P_1(k_s, \theta_S)$ for $\theta_c = 5^\circ,\ 25^\circ$, and $\Delta\theta = 2^\circ$. Profiles are ploted as a function of θ_S, with different curves corresponding to $k_S = 0, .., \langle k_L \rangle /10$ (curves with larger P_1 values correspond to larger k_S).

Fig. 5.— Diffusive decay: dimensionless factor $P_1(k_s, \theta_S)$ for $\theta_c = 0.5^\circ$ and $\Delta\theta = 0.5^\circ$. Profiles are ploted as a function of θ_S, with different curves corresponding to $k_S = 0, .., \langle k_L \rangle /10$ (curves with larger P_1 values correspond to larger k_S).

Fig. 6.— Diffusive decay: for a fixed $k_S = \langle k_L \rangle /10$, dimensionless factor $P_1(k_s, \theta_S)$ for $\theta_c = 5^\circ,\ 25^\circ$, and $\Delta\theta = 2^\circ,\ 10^\circ$. Profiles are ploted as a function of θ_S, with thin curve corresponding to $\Delta\theta = 2^\circ$ and thick curve to $\Delta\theta = 10^\circ$.

Fig. 7.— Back-scattering: dimensionless factor $P_1(k_s, \theta_S)$ for $\theta_c = 5^\circ,\ 25^\circ$, and $\Delta\theta = 2^\circ$. Profiles are ploted as a function of θ_S, with thin curves corresponding to $k_S = 2k_{L,min} - 2k_0$ and thick curves to $k_S = 2k_{L,max} - 2k_0$.

Fig. 8.— Back-scattering: dimensionless factor $P_1(k_s, \theta_S)$ for $\theta_c = 0.5^\circ$ and $\Delta\theta = 0.5^\circ$. Profiles are ploted as a function of θ_S, with thin curves corresponding to $k_S = 2k_{L,min} - 2k_0$ and thick curves to $k_S = 2k_{L,max} - 2k_0$.

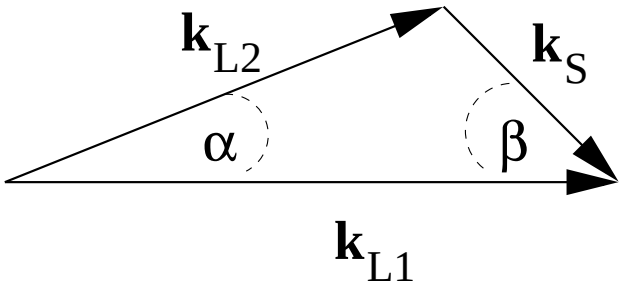
$\mathbf{k}_{L2}$
$\mathbf{k}_S$
α
β
$\mathbf{k}_{L1}$

Fig. 1.—

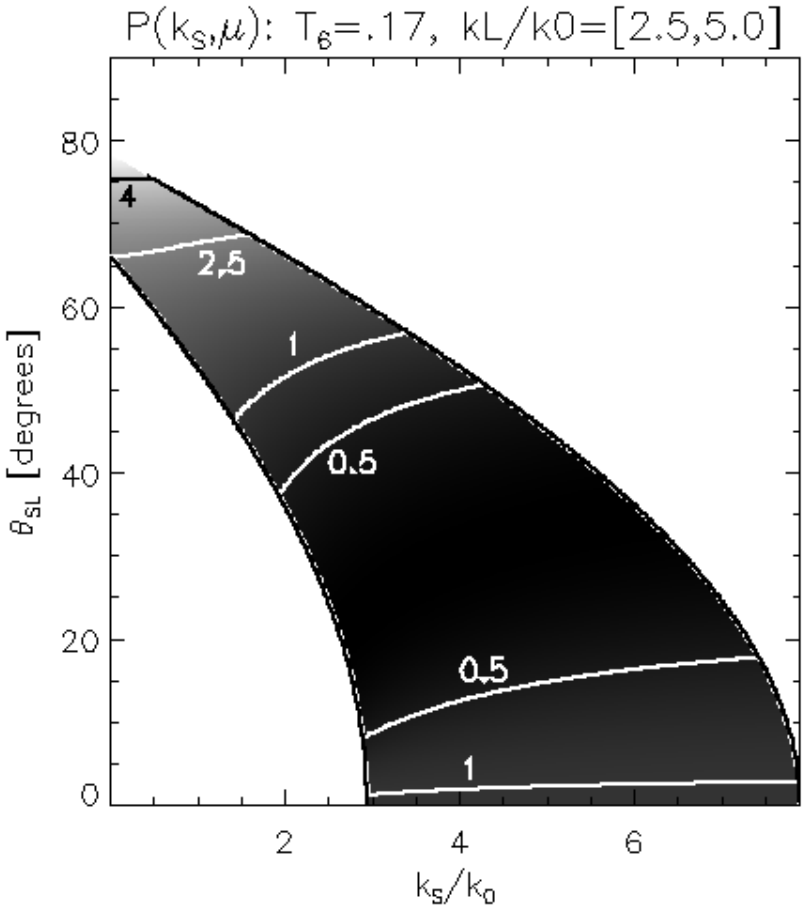
P(k_S,μ): T_6=.17, kL/k0=[2.5,5.0]
80
60
40
20
0
θ_SL [degrees]
2
4
6
k_S/k_0
4
2.5
1
0.5
0.5
1

Fig. 2.—

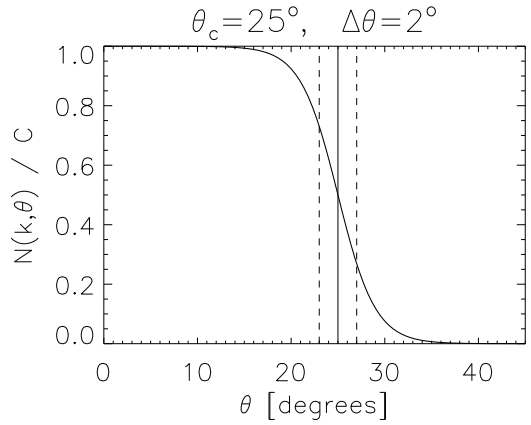

Fig. 3.—

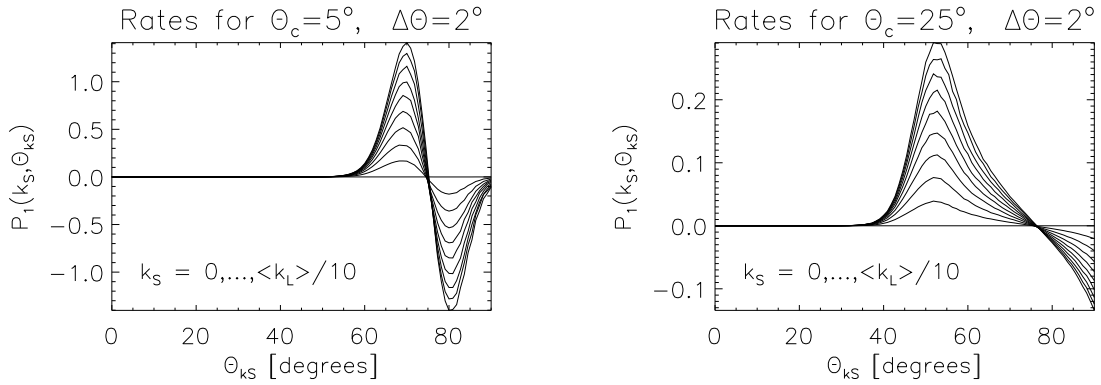

Fig. 4.—

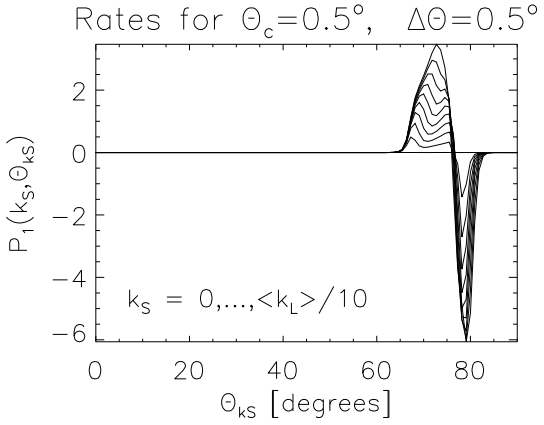

Fig. 5.—

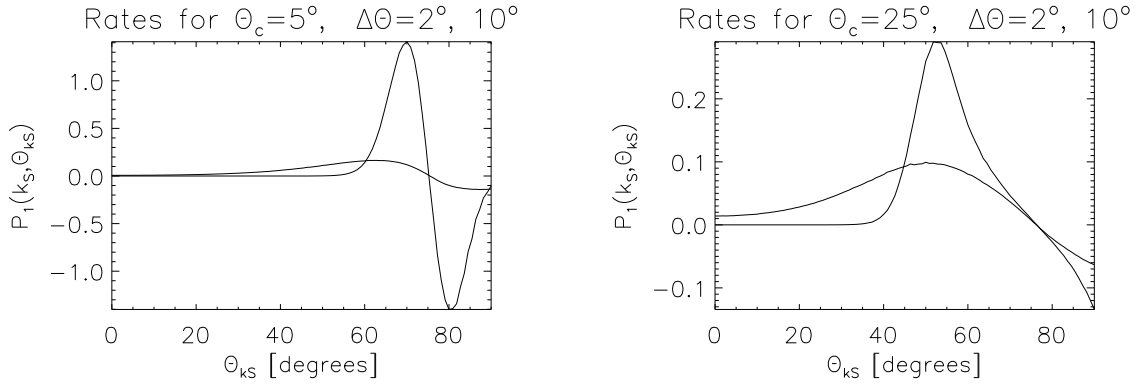

Fig. 6.—

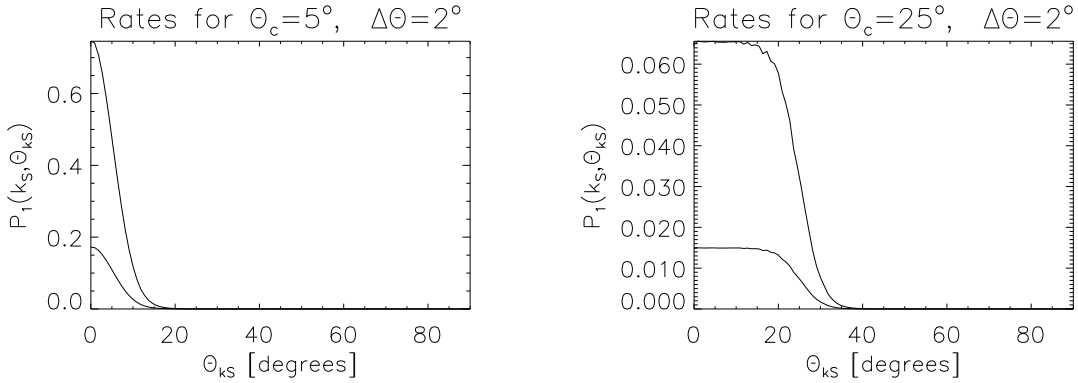

Fig. 7.—

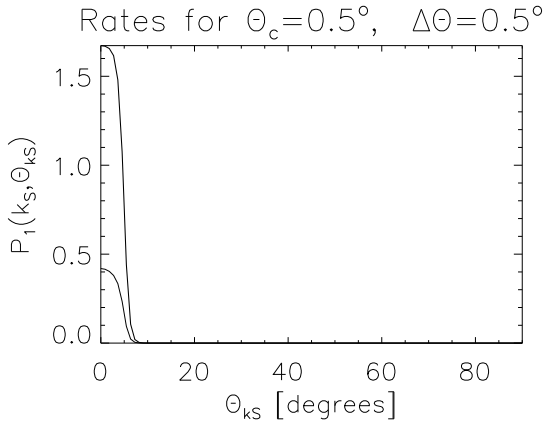

Fig. 8.—